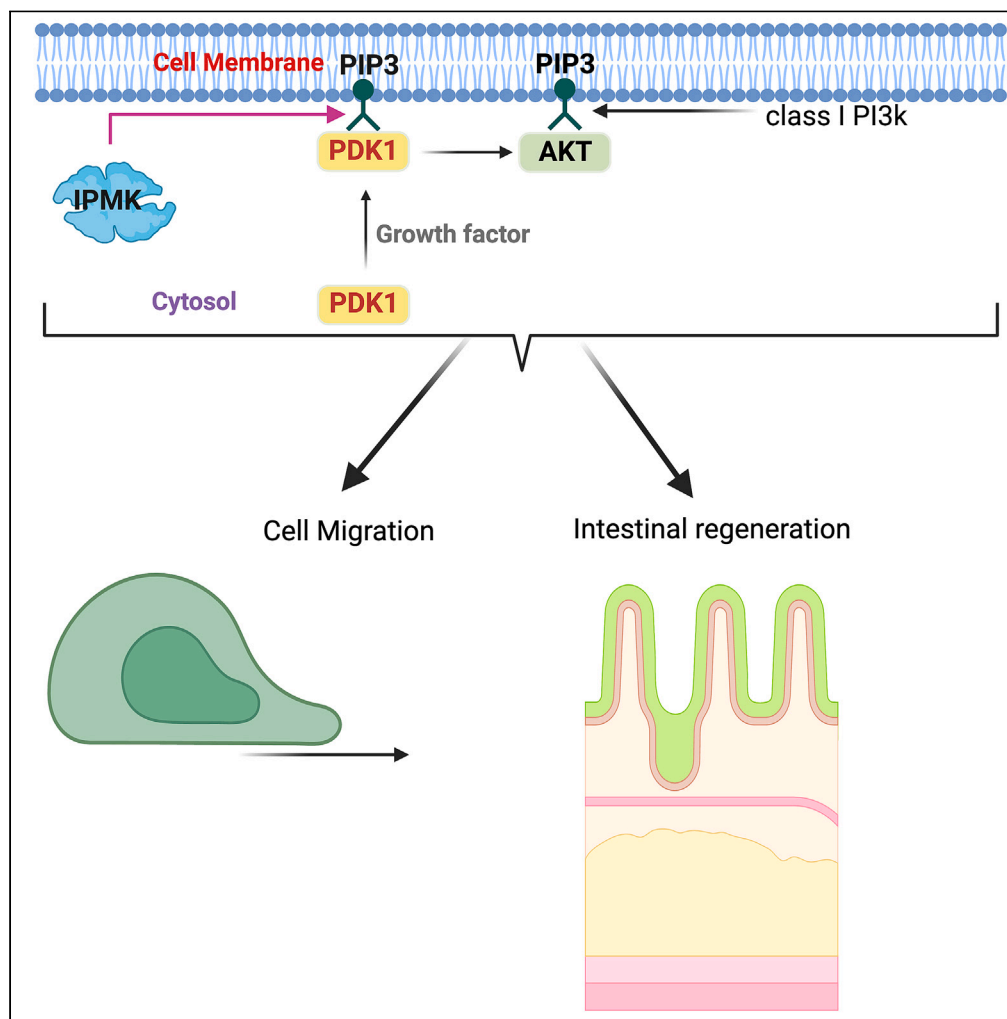


Article

Loss of PI3k activity of inositol polyphosphate multikinase impairs PDK1-mediated AKT activation, cell migration, and intestinal homeostasis



Luke Reilly, Evan R. Semenza, George Koshkaryan, ..., Mark Donowitz, Solomon H. Snyder, Prasun Guha

ssnyder@jhmi.edu (S.H.S.)
prasun.guha@unlv.edu (P.G.)

Highlights

PI3k activity of IPMK is critical for PDK1 membrane localization

IPMK is important for AKT activation

IPMK is crucial for cell migration

IPMK is linked to intestinal regeneration/Paneth cell organization

Reilly et al., iScience 26, 106623
May 19, 2023 © 2023 The Author(s).
<https://doi.org/10.1016/j.isci.2023.106623>



Article

Loss of PI3k activity of inositol polyphosphate multikinase impairs PDK1-mediated AKT activation, cell migration, and intestinal homeostasis

Luke Reilly,¹ Evan R. Semenza,¹ George Koshkaryan,⁹ Subrata Mishra,^{7,8} Sujan Chatterjee,⁹ Efrat Abramson,² Pamela Mishra,¹¹ Yoshitatsu Sei,³ Stephen A. Wank,³ Mark Donowitz,⁴ Solomon H. Snyder,^{1,5,6,*} and Prasun Guha^{1,9,10,12,*}

SUMMARY

Protein kinase B (AKT) is essential for cell survival, proliferation, and migration and has been associated with several diseases. Here, we demonstrate that inositol polyphosphate multikinase (IPMK's) lipid kinase property drives AKT activation via increasing membrane localization and activation of PDK1 (3-Phosphoinositide-dependent kinase 1), largely independent of class I PI3k (cPI3K). Deletion of IPMK impairs cell migration, which is partially associated with the abolition of PDK1-mediated ROCK1 disinhibition and subsequent myosin light chain (MLC) phosphorylation. IPMK is highly expressed in intestinal epithelial cells (IEC). Deleting IPMK in IEC reduced AKT phosphorylation and diminished the number of Paneth cells. Ablation of IPMK impaired IEC regeneration both basally and after chemotherapy-induced damage, suggesting a broad role for IPMK in activating AKT and intestinal tissue regeneration. In conclusion, the PI3k activity of IPMK is necessary for PDK1-mediated AKT activation and intestinal homeostasis.

INTRODUCTION

Inositol polyphosphates are signaling molecules generated by an evolutionarily conserved family of kinases. Inositol 1,4,5-trisphosphate (IP₃) is well established as a physiologic regulator of intracellular calcium.¹ Among the family of kinase enzymes regulating inositol phosphates, IPMK is notable for its generation of multiple inositol phosphates, including inositol tetrakisphosphate (IP₄) and inositol pentakisphosphate (IP₅).² Additionally, IPMK serves as a phosphoinositide 3-kinase (PI3k) in mammalian cells.³ The PI3k activity of IPMK, like that of cPI3k enzymes, contributes to AKT activation.³ Independent of its kinase activity, IPMK mediates autophagy by binding to AMP-dependent protein kinase and the autophagy-activating kinase ULK1.⁴ IPMK also participates in nutrient sensing and activation of mTORC1 and mTORC2.⁵ Epidemiological studies indicate that the mutation of IPMK at its nuclear localization signal is associated with familial intestinal carcinoids.⁶ Genome-wide association study (GWAS) data from patients with inflammatory bowel disease (IBD) have established IPMK as a putative risk gene.⁷

AKT is a central player in the regulation of metabolism, cell survival, motility, transcription, and cell-cycle progression.⁸ cPI3k (p110 α , β , γ , and δ) generates the second messenger phosphatidylinositol (3,4,5)-trisphosphate (PIP₃) from phosphatidylinositol (4,5)-bisphosphate (PIP₂). PIP₃ production stimulates the translocation of AKT from the cytoplasm to the plasma membrane, an action that requires its pleckstrin homology (PH) domain. The serine/threonine kinase phosphoinositide-dependent kinase 1 (PDK1) also contains a PH domain and is recruited to the plasma membrane by PIP₃. PDK1 phosphorylates AKT at Thr308,⁸ while phosphorylation at Ser473 is mediated by mTORC2.⁹ Phosphorylation of AKT at both Thr308 and Ser473 generates an active form of AKT, which targets specific proteins in the cytoplasm and nucleus. Several lines of evidence suggest that cPI3k is not the critical enzyme for recruiting PDK1 and mTORC2 to the membrane to activate AKT.^{10–12} PIP₃-mediated PDK1 membrane localization is also crucial for the activation of Rho-associated coiled-coil-containing kinase 1 (ROCK1), an essential mediator of cell migration. PDK1-mediated ROCK1 activation appears to be only marginally influenced by the inhibition of cPI3k,^{12,13} suggesting a different PI3k mediates this effect. We previously showed that the deletion of IPMK abolishes the activation of AKT³ via heretofore obscure mechanisms. Here we

¹The Solomon H. Snyder Department of Neuroscience, Johns Hopkins University School of Medicine, Baltimore, MD 21205, USA

²Department of Neurology, Johns Hopkins University School of Medicine, Baltimore, MD 21205, USA

³Digestive Diseases Branch, National Institute of Diabetes and Digestive and Kidney Diseases, National Institutes of Health, Bethesda, MD, USA

⁴Department of Medicine, Division of Gastroenterology, Johns Hopkins University School of Medicine, 720 Rutland Avenue, Baltimore, MD 21205, USA

⁵Department of Psychiatry and Behavioral Sciences, Johns Hopkins University School of Medicine, Baltimore, MD 21205, USA

⁶Department of Pharmacology and Molecular Sciences, Johns Hopkins University School of Medicine, Baltimore, MD 21205, USA

⁷Department of Biophysics and Biophysical Chemistry, Johns Hopkins University School of Medicine, Baltimore, MD 21205, USA

⁸Reference Standard Laboratory, United States Pharmacopeial Convention, Rockville, MD 20852, USA

⁹Nevada Institute of Personalized Medicine (NIPM), University of Nevada, Las Vegas, NV 89154, USA

¹⁰School of Life Sciences, University of Nevada, Las Vegas, NV 89154, USA

¹¹Marie-Josée and Henry R. Kravis Center for Molecular Oncology, Memorial Sloan

Continued



demonstrate that IPMK is the principal PI3k regulating PDK1's membrane localization and associated AKT activation and ROCK1-mediated cell migration. We further show that IPMK physiologically influences the self-renewal of the intestinal epithelium.

RESULTS

Inositol polyphosphate multikinase -mediated AKT activation is independent of cPI3k

Previously, we showed that IPMK is a novel eukaryotic PI3kinase, and deletion of IPMK impairs the activation of AKT.³ Here we investigated the physiological importance of IPMK as a lipid kinase and its detailed mechanism of AKT activation. To determine the contribution of IPMK to the total cellular PIP₃ pool, we used a PIP₃ Mass ELISA kit. Using IPMK WT/KO MEFs, we found that overnight serum starvation markedly diminished intracellular PI (3,4,5) P₃ levels in both WT/KO cells (Figures 1 and S1F). PIP₃ is rapidly produced with in 5 min of serum treatment. Deletion of IPMK diminished the PIP₃ level by around 44.9%. The inhibition of cPI3k with two selective inhibitors, Pictilisib (GDC0941, a pan cPI3k inhibitor with the highest selectivity at the concentration of 3-33 nM *in vitro* and used in clinical trial phase Ib) and LY294002, reduced PIP₃ level by 58% in WT cells. Interestingly, even after cPI3k inhibitor (cPI3ki) treatment, WT cells retain almost 42% of PIP₃, implying the presence of a cPI3k independent PIP₃ pool (Figure 1A). IPMK KO cells treated with cPI3ki had further reduced PIP₃ levels which were comparable to serum-starved cells (Figure 1A). This suggests lipid kinases generating PIP₃ in IPMK KO cells are sensitive to cPI3ki. Intracellular PIP₂ levels were comparable in WT/KO cells (Figure S1A), demonstrating that the production of PIP₃ in IPMK KO cells was not influenced by the PIP₂ pool.

To examine whether loss of IPMK diminished PIP₃ production in primary cells, we generated the intestinal deletion of IPMK (*Ipmk*^{ΔIEC}) as IPMK is highly enriched in intestinal crypts (Figures 1B and S1F). We purified primary crypts to perform the enteroid culture. Consistent with MEF data, PIP₃ production was substantially reduced in *Ipmk*^{ΔIEC} crypt compared to *Ipmk*^{F/F}, suggesting that PI3kinase activity of IPMK is essential for PIP₃ production in primary intestinal enteroid cells (Figure 1B). Intracellular PIP₂ levels were comparable in *Ipmk*^{F/F}/*Ipmk*^{ΔIEC} cells (Figure S1B).

To delineate the biological importance of the lipid kinase activity of IPMK, it is critical to understand the influence of cPI3k or PI3k on IPMK's lipid kinase activity. Previously, Resnick et al.¹⁴; showed that recombinant rat and yeast IPMK protein purified from untreated cells was insensitive to wortmannin treatment. However, Maag et al.³ showed that IPMK purified from wortmannin-treated cells partially lost its PI3kinase activity, but was ineffective when treated *in vitro*, directly in an IPMK's lipid kinase reaction. Later it was discovered that wortmannin is not a specific cPI3ki, and it directly inhibits multiple essential kinases such as ATM, ATR, MLCK, and so forth,¹⁵ which may have off-target severe effects when treated in cell lines.

To determine the influence of cPI3ki on IPMK, we overexpressed myc-IPMK in HeLa cells, followed by immunoprecipitation using myc agarose beads to perform *in vitro* PI3kinase activity assay of IPMK (Figure 1C). Interestingly, IPMK purified from pictilisib-treated cells completely retained its PI3kinase activity, insinuating that cPI3k does not influence IPMK's lipid kinase property (Figure 1C). Furthermore, we purified IPMK and p85 from untreated cells and incubated immunocomplex with Pictilisib *in vitro*. As expected, treatment with Pictilisib markedly diminished PI3kinase activity of the p85 immunocomplex, whereas there was no effect on IPMK's PI3kinase activity even at the high dose of 5 μM (Figure 1C). IPMK purified from serum-starved cells also showed substantial PI3kinase activity, implying that serum or growth factor stimulation mediated posttranslational modification on IPMK is important for its lipid kinase activity in the cellular system but not essential for its *in vitro* kinase activity (Figure 1C). Previous studies demonstrated that other PI3kinase inhibitors, such as LY294002 and Wortmannin, do not influence IPMK's lipid kinase activity *in vitro*,¹⁴ which agrees with our present finding and confirms that the lipid kinase activity of IPMK is independent of cPI3ki.

To ascertain the influence of IPMK on the lipid kinase activity of cPI3k, we immunoprecipitated the p85/p110 complex from IPMK WT and IPMK KO MEFs, followed by analyzing the lipid kinase activity of cPI3k using a PI3kinase activity ELISA. Intriguingly, p85/p110 immunocomplex purified from IPMK KO MEFs and WT cells displayed comparable activity, confirming that cPI3k activity is independent of IPMK (Figure S1C).

Overall, the above data conclude that IPMK is a physiological PI3kinase, and its lipid kinase activity is independent of cPI3k and entirely unresponsive to cPI3ki.

Kettering Cancer Center,
New York City, NY, USA

¹²Lead contact

*Correspondence:
ssnyder@jhmi.edu (S.H.S.),
prasun.guha@unlv.edu (P.G.)
<https://doi.org/10.1016/j.isci.2023.106623>

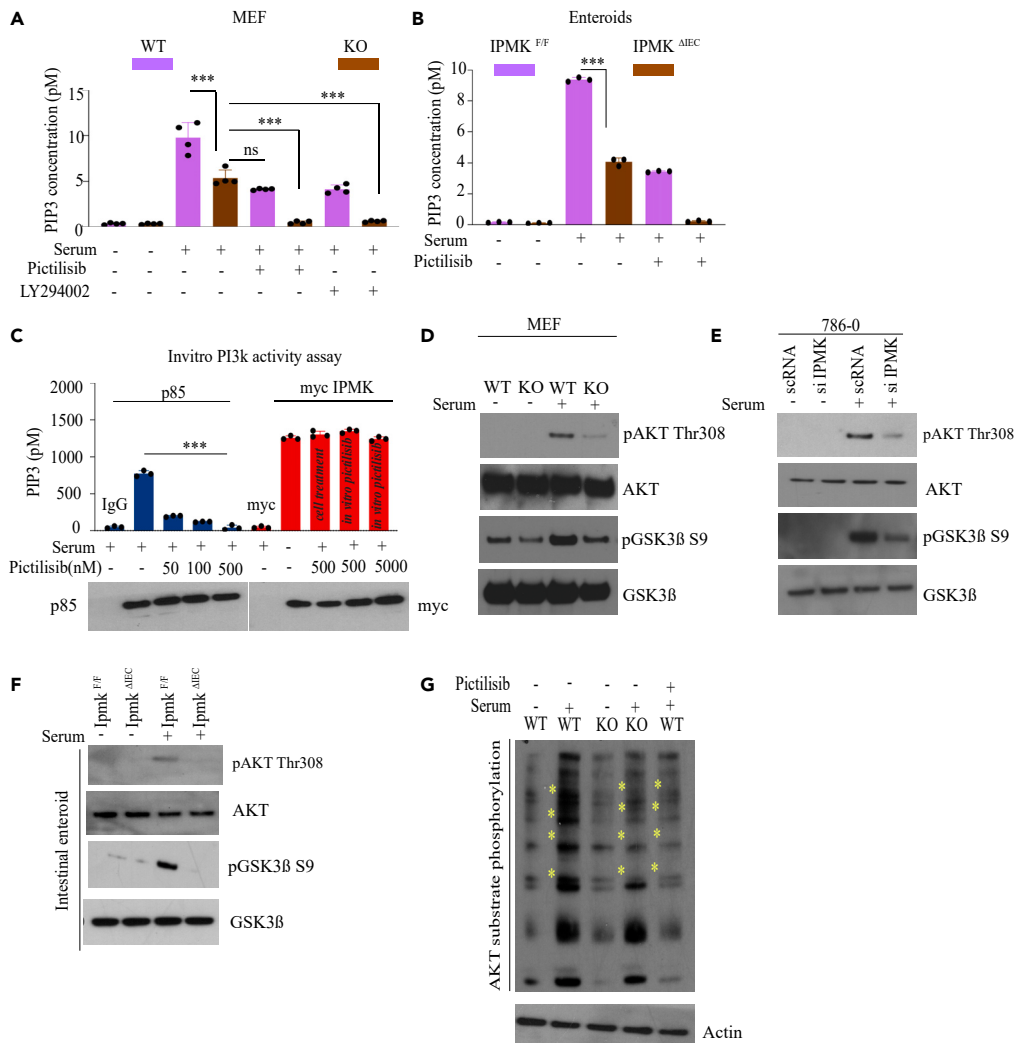


Figure 1. IPMK mediates AKT activation

(A) Total PIP₃ concentration in MEF cells by PIP₃ ELISA. ***p < 0.001. Data are graphed as mean ± SD.
 (B) PIP₃ concentration in intestinal enteroids by PIP₃ ELISA. ***p < 0.001. Data are graphed as mean ± SD.
 (C) P85 and myc IPMK were immunoprecipitated and used *in vitro* PI3k assays by ELISA. Immunoblot of p85 and myc to confirm the total amount of protein immunoprecipitated. Pictilisib treatment in different doses (nM). ***p < 0.001. Data are graphed as mean ± SD.
 (D) Western blot of AKT (Thr308) and GSK3β (Ser9) phosphorylation in serum-starved WT and IPMK KO MEFs with or without serum stimulation for 5 min. (n=3).
 (E) Western blot of AKT (Thr308) and GSK3β (Ser9) phosphorylation in 786-0 cells after knocking down IPMK by siRNA. (n=3).
 (F) Western blot of AKT (Thr308) and GSK3β (Ser9) phosphorylation in intestinal enteroids. (n= 3).
 (G) Western blot of phosphorylated AKT substrates in WT and IPMK KO MEFs treated with serum or pictilisib (100 nM, 30 min). (n= 3).

Activation of AKT is highly regulated by PIP₃ production.¹⁶ PDK1 and mTORC2 are two major kinases phosphorylating AKT at Thr308 and Ser473, respectively.¹⁶ We previously showed that IPMK directly promotes mTORC2 activation⁵ and thus may impair AKT Ser473 phosphorylation (Figures S1D and S1E). Here, we explored mechanisms underlying deficits in AKT Thr308 phosphorylation in *Ipmk*-deleted cells. In agreement with the previous study,³ we found that *Ipmk* deletion markedly diminished AKT phosphorylation at Thr308 in MEF (Figures 1D and S1F). We extended our findings to other cell lines. Depletion of IPMK in 786-0 (a renal cancer cell lines) substantially reduced AKT Thr308 phosphorylation (Figures 1E and S1F). Next, we analyzed the effects of IPMK loss in intestinal enteroid culture. Deletion of IPMK markedly

diminished AKT Thr308 phosphorylation in *lpmk*^{dIEC} enteroids compared to *lpmk*^{F/F} (Figures 1F and S1F), suggesting a cell line independent influence of IPMK on AKT Thr308 phosphorylation. AKT phosphorylates GSK3 β at Ser9 to inactivate GSK3 β .⁸ IPMK KO MEFs showed a substantial loss of GSK3 β phosphorylation at Ser9 in all experimental cell types (Figures 1D–1F). To determine whether the phosphorylation of other AKT substrates might be defective in IPMK-deleted cells, we used an antibody that recognizes proteins containing phosphorylated AKT substrate domains.¹⁷ Phosphorylation detected by this antibody was considerably reduced in IPMK KO MEFs and comparable to cells treated with the pan-cPI3ki pictilisib (Figure 1G).

Hence, we conclude that the lipid kinase activity of IPMK is independent of cPI3k and is critical for AKT activation.

PI3k activity of inositol polyphosphate multikinase is required for the activation of AKT but not AKT membrane localization

To ascertain the importance of IPMK's catalytic activity (Figure 2A) in regulating AKT phosphorylation, we rescued IPMK KO MEFs with stable overexpression of WT or kinase-dead (KSA) IPMK and *Arabidopsis* IPMK (IPK2 β).³ We previously showed that IPK2 β possesses only inositol kinase property but lacks lipid kinase activity.³ IPK2 β fails in rescuing AKT Thr308 activation, confirming that the PI3kinase activity of IPMK is essential for AKT Thr308 phosphorylation (Figure 2B).

PIP₃ promotes AKT membrane localization and subsequent activation.⁸ To investigate the role of IPMK in growth factor-stimulated membrane localization of AKT, we overexpressed the AKT PH domain fused to GFP in WT and IPMK KO MEFs. Serum stimulation efficiently promoted GFP-AKT-PH membrane translocation in WT and KO cells (Figures 2C and 2D). By contrast, GFP-AKT-PH membrane localization was prevented by treatment with pictilisib (pan-cPI3ki). These immunocytochemical results were further confirmed by cell fractionation and western blotting of AKT in the cytoplasmic and membrane fractions after serum stimulation (Figure 2E). To confirm that IPMK-independent AKT membrane localization is not cell type-specific, we performed a cell fractionation study in the 786-0 cell line. After serum treatment, the transient knockdown of IPMK in 786-0 cells failed to impair AKT membrane localization but was markedly inhibited by pictilisib (Figures S2A and S2B). Thus, the PI3kinase activity of IPMK is essential for AKT Thr308 phosphorylation but dispensable for AKT membrane localization.

PI3k activity of inositol polyphosphate multikinase mediates PDK1 membrane localization

PDK1 is the essential AKT-kinase that phosphorylates AKT at Thr308.⁸ Growth factors stimulate PDK1 membrane recruitment and phosphorylation of AKT.⁸ We wondered whether IPMK directly stimulates the kinase activity of PDK1. PDK1 autophosphorylation at Ser 241 is necessary for PDK1's kinase activity.¹⁸ Depletion of IPMK in MEF failed to impair PDK1 Ser 241 phosphorylation (Figure 3A). To directly study the influence of IPMK on PDK1 kinase activity, we pulled down PDK1 from WT and KO MEFs and performed an *in vitro* kinase assay using AKT as a substrate. Deletion of IPMK did not impact PDK1-mediated AKT phosphorylation *in vitro* (Figure S3A). Thus, IPMK has no direct influence on PDK1 kinase activity.

Serum or growth factor stimulation promotes the generation of PIP₃, which binds to the PH domain of PDK1, translocating a fraction of PDK1 from the cytoplasm to the cell membrane.¹⁰ By contrast, inositol phosphate is not required for such action. At the membrane, PDK1 acts as an AKT kinase, phosphorylating AKT at Thr308.⁸

We hypothesized that IPMK-derived PIP₃ might influence PDK1 membrane localization. WT and KO MEFs were transiently transfected with full-length GFP-PDK1, followed by overnight serum starvation. As expected, treatment with serum induced the export of PDK1 to the cell membrane in WT MEFs, an action that was abolished in IPMK KO cells (Figures 3B and 3C). By contrast, pictilisib had only a marginal effect on PDK1 membrane localization (Figures 3D and 3E). We confirmed these microscopy data by western blotting of PDK1 from cytoplasmic and membrane fractions with or without serum stimulation (Figures 3F and 3G). Transient depletion of IPMK in 786-0 cells also inhibited PDK1 membrane localization, but was only slightly influenced by pictilisib (Figure S3B). The above data suggest that IPMK is the primary PI3k regulating PDK1 membrane localization.

To ascertain the importance of IPMK's catalytic activity in regulating PDK1 membrane localization, we performed a western blot of PDK1 in cytoplasmic and membrane fractions from IPMK KO MEFs stably

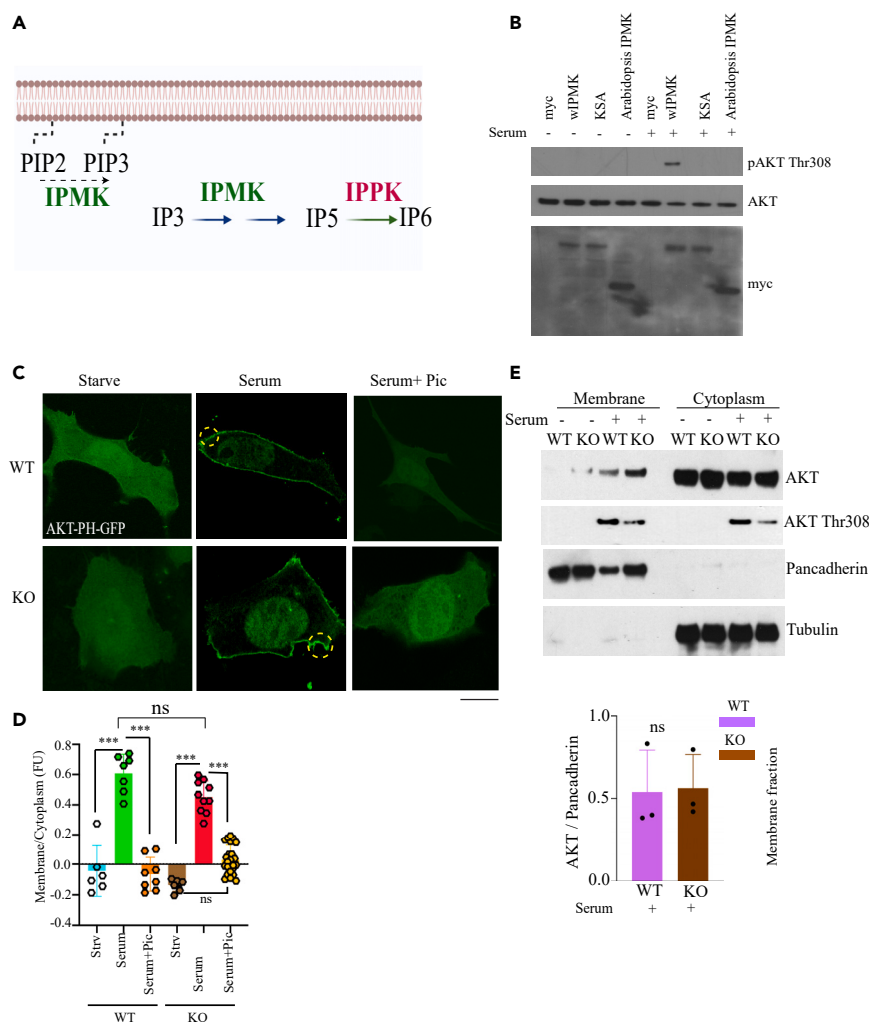


Figure 2. PI3k activity of IPMK is required for the activation of AKT

(A) Schematic diagram of IPMK enzymatic pathway.

(B) Western blot of AKT Thr308 phosphorylation in response to serum stimulation in IPMK KO MEFs stably overexpressing myc-tagged empty vector (myc), WT IPMK (WT), or kinase dead IPMK (KSA) and Arabidopsis IPMK.

(C) AKT-PH-GFP transfected in IPMK WT/KO MEF and performed confocal imaging for AKT-PH-GFP membrane localization. Scale bar 20 μ m. Membrane-localized AKT-PH-GFP is marked by a yellow circle.

(D) The bar diagram shows the relative AKT-PH-GFP membrane/cytoplasm fluorescence ratio. ***p < 0.001. Data are graphed as mean \pm SD.

(E) The cell fractionation study to understand endogenous AKT membrane localization in MEFs. Pancadherin is the marker for cell membrane fraction, and tubulin for the cytosolic fraction. ns = not significant.

overexpressing empty vector (myc), WT IPMK, KSA or IPK2 β . PDK1 membrane localization was evident in cells rescued with WT IPMK but was absent in cells rescued with either empty vector, KSA or IPK2 β (*Arabidopsis* IPMK) (Figure 3H), confirming that the lipid kinase activity of IPMK is required for PDK1 membrane localization.

PDK1 membrane localization is also known to impair ROCK1/RhoE binding, resulting in ROCK1 activation, phosphorylation of myosin light chain (MLC), and cell migration.^{12,13} Previous studies¹² showed that PIP₃ promotes the localization of PDK1 to the cell membrane, where it dissociates the ROCK1-inhibiting RhoE from ROCK1, with effects only modestly impacted by cPI3ki. We examined the influence of IPMK upon ROCK1/RhoE binding by the immunoprecipitation of ROCK1. RhoE/ROCK1 interactions were equal under serum starvation conditions in WT and KO MEFs. Stimulation with serum for 5 min markedly depleted ROCK1 binding to RhoE in WT cells, whereas KO cells maintained the ROCK1/RhoE complex at levels comparable to serum starvation (Figure S3C). Myosin light chain (MLC) is a downstream substrate of ROCK1,¹³

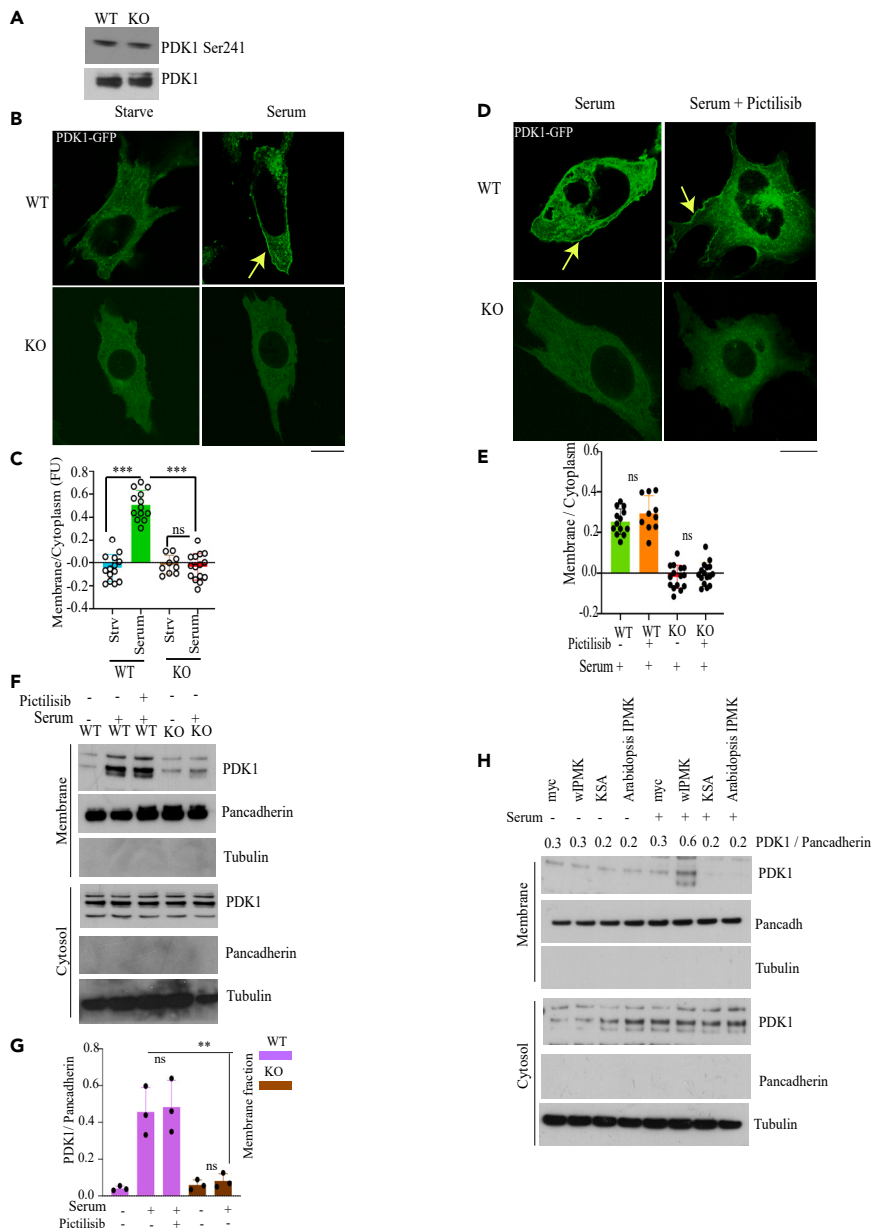


Figure 3. PI3k activity of IPMK mediates PDK1 membrane localization

(A–E) Western blot of PDK1 Ser 241 in MEFs. Staining (B and D) (yellow arrow indicates membrane localized PDK1-GFP) and quantification (C is the quantification of B and E is the quantification of D) of overexpressed PDK1-GFP subcellular localization in IPMK WT and KO MEFs with or without serum stimulation and cPI3ki pictilisib. Membrane-localized PDK1-GFP is marked by the yellow arrow. Scale bar 20 μ m. The bar graph shows the relative PDK1-GFP membrane/cytoplasm fluorescence ratio. ***p < 0.001. Data are graphed as mean \pm SD.

(F and G) Western blot of endogenous PDK1 in cytoplasmic and membrane fractions isolated from WT and IPMK KO MEFs in response to serum stimulation. Pan-cadherin and tubulin blots confirm the purity of membrane and cytoplasm fractions, respectively. Data are graphed as mean \pm SD. **p < 0.05, ns = not significant.

(H) The cell fractionation study for PDK1 membrane localization for IPMK KO MEFs rescued with myc, wild-type IPMK, KSA, and *Arabidopsis* IPMK.

and phosphorylation MLC promotes cell migration by modulating actin polymerization.^{12,13} Deletion of IPMK markedly reduced MLC phosphorylation (Figure S3D) and cell migration (Figure S3E). These data further confirm that IPMK promotes PDK1 membrane localization and its downstream signaling events.

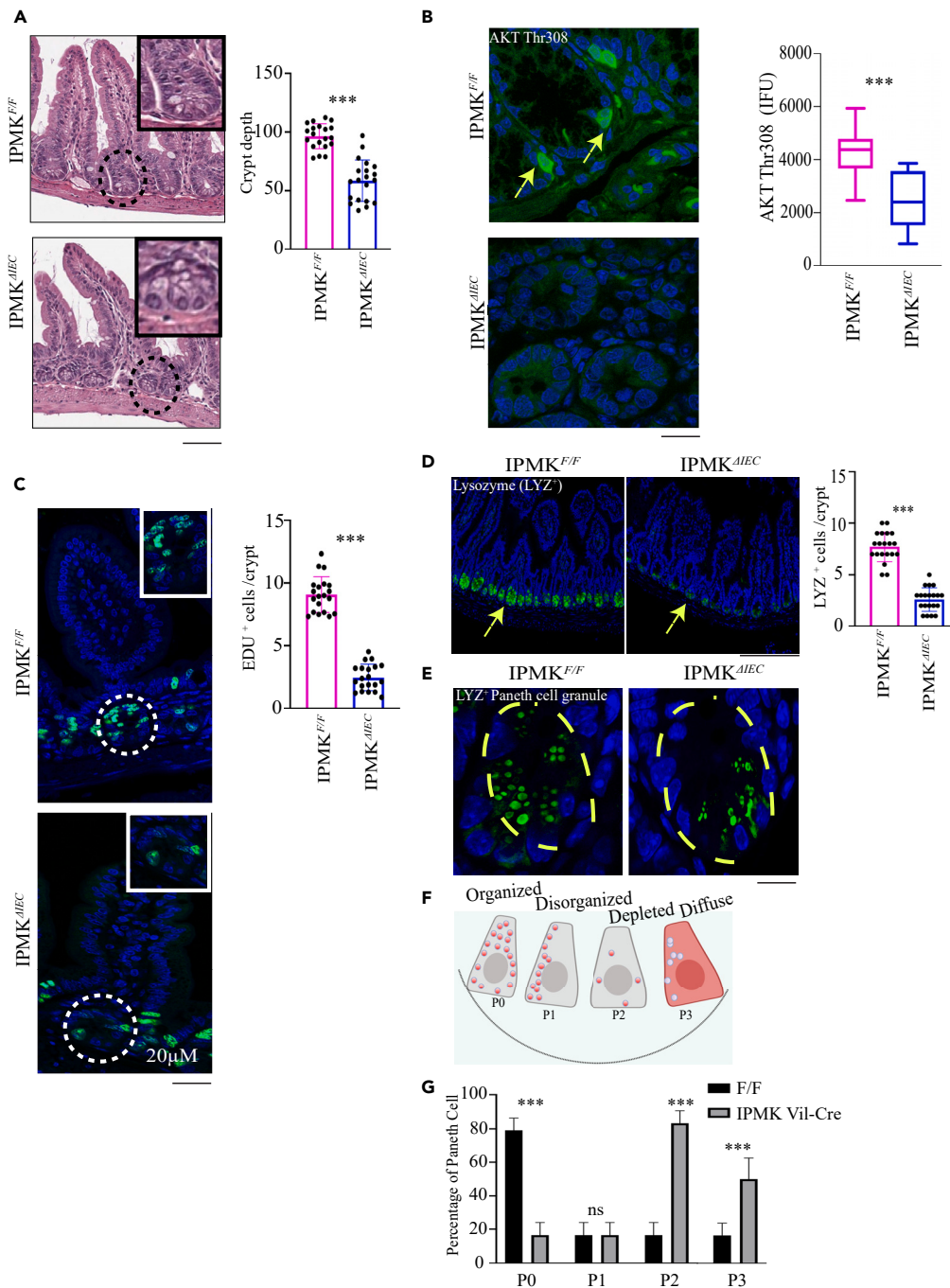


Figure 4. IPMK is essential for intestinal integrity

(A) H&E staining of ileum sections from *Ipmk*^{F/F} and *Ipmk*^{ΔIEC} mice. The graph depicts crypt depth. n = 4 mice each group, ***p < 0.001. The black circle is the crypt shown in a magnified view (black square). Data are graphed as mean ± SD. Scale bar 200 μm.

(B) AKT Thr308 staining (green) of ileum sections from *Ipmk*^{F/F} and *Ipmk*^{ΔIEC} mice, n = 4 mice in each group. ***p < 0.001. Data are graphed as mean ± SD. DAPI (blue) was used for nuclear staining. The yellow arrow indicates AKT Thr308 staining. Scale bar 10 μm.

(C) EdU (green) staining in intestinal sections from *Ipmk*^{F/F} and *Ipmk*^{ΔIEC} mice intraperitoneally injected with EdU 2h prior to sacrifice. DAPI (blue) was used for nuclear staining. The white circle is the crypt shown in a magnified view (white square). The number of EdU-positive cells were counted, n = 4 mice in each group. ***p < 0.001. Data are graphed as mean ± SD. Scale bar 20 μm.

Figure 4. Continued

(D and E) Paneth cell granules were identified by lysozyme (LYZ) staining (green) in ileum sections from *Ipmk^{F/F}* and *Ipmk^{ΔIEC}* mice, n = 4 mice in each group. ***p < 0.001. (D) is the low magnification (20× air) image scale bar 50 μm. The yellow arrow indicates LYZ positive crypts, and (E) is a high magnification (60× oil) image scale bar 10 μm. The yellow circle shows the Paneth cell in the side crypt. Data are graphed as mean ± SD. DAPI (blue) was used for nuclear staining. (F and G) Cartoon (F) and quantification (G) of lysosomal granule distribution in Paneth cells in *Ipmk^{F/F}* and *Ipmk^{ΔIEC}* ileum sections. n = 4 mice in each group. ***p < 0.001. Data are graphed as mean ± SD.

Inositol polyphosphate multikinase is essential for intestinal integrity

Previous RNA *in situ* hybridization studies established high IPMK expression in the intestinal ileum.⁶

To investigate a potential role for IPMK in the activation of AKT and intestinal homeostasis, we crossed *Ipmk* floxed mice (*Ipmk^{F/F}*) with *Villin-Cre* mice to generate a mouse line lacking *Ipmk* selectively in intestinal epithelial cells (IECs) (*Ipmk^{ΔIEC}*) (Figure S1F). *Ipmk^{ΔIEC}* mice were born at the expected Mendelian ratios and developed normally. IEC-specific deletion of *Ipmk* in 8 to 12-weeks old mice resulted in decreased crypt depth in the ileum (Figure 4A). Cell proliferation in the intestinal epithelium, one of the most proliferative tissues in mammals, requires the activation of AKT.¹⁹ *Ipmk^{F/F}* mice showed prominent AKT Thr308 staining, which was markedly diminished in *Ipmk^{ΔIEC}* mice (Figure 4B), demonstrating that IPMK is a physiological regulator of AKT *in vivo*.

Next, we examined the importance of IPMK in IEC proliferation under basal conditions. *Ipmk*-deleted IECs showed a marked loss of incorporation of 5-ethynyl-2'-deoxyuridine (EdU), a thymidine analog that is incorporated into the DNA of proliferative cells, suggesting that IPMK is critical for IEC proliferation (Figure 4C). To further examine the effect of IPMK deletion on intestinal proliferation, we cultured enteroids isolated from *Ipmk^{F/F}* and *Ipmk^{ΔIEC}* small intestines. After 7 days of culture, enteroids from *Ipmk^{F/F}* mice showed proper budded structure, while *Ipmk^{ΔIEC}* enteroids showed less morphological complexity (Figures S4A and S4B). Culture of an equal initial number of cells from *Ipmk^{ΔIEC}* mice gave rise to fewer enteroids than cells cultured from *Ipmk^{F/F}* mice (Figure S4B). To ascertain the effect of AKT and PDK1 on the proliferation of enteroids, we incubated *Ipmk^{F/F}* enteroids for 7 days with specific AKT and PDK1 inhibitors. AKT and PDK1 inhibitors both phenocopied IPMK deletion, reducing the enteroid abundance and producing enteroids with deformed structure (Figures S4A and S4B). AKT is a master regulator of cell proliferation and can play this role through multiple mechanisms. In IECs, phosphorylation of β-catenin at Ser552 by AKT elicits its translocation to the nucleus, where β-catenin acts as a transcriptional coactivator to stimulate cellular proliferation.²⁰ Nuclear localization of β-catenin Ser 522 was notably reduced in *Ipmk^{ΔIEC}* mice at the intestinal crypt base (Figure S4C), which was further validated by western blot from enteroid (*Ipmk^{F/F}*/*Ipmk^{ΔIEC}*) lysates (Figure S4C). Wnt 3A signaling upstream of β-catenin is directly related to intestinal regeneration. We wondered about the influence of IPMK for Wnt 3A dependent gene expressions. Axin2, c-Myc, and Lef1 are important Wnt3A-dependent genes critical for intestinal homeostasis.²¹ Interestingly IPMK depletion considerably impaired Axin2 protein expression while c-Myc and Lef1 expression in IPMK KO MEF cells were comparable to the WT (Figure S4D). Axin 2 protein expression in *Ipmk^{ΔIEC}* enteroids was also reduced compared to *Ipmk^{F/F}* confirming the cell line data (Figure S4E). This indicates that IPMK is critical for Wnt 3A-mediated Axin2 expression; however, a more in-depth examination of the significance of IPMK on canonical Wnt signaling activation in intestinal regeneration will be conducted in a future study.

Activation of AKT is essential for the homeostasis of Paneth cells, specialized crypt-resident cells that support intestinal regeneration by maintaining intestinal stem cell homeostasis.²² Intestinal deletion of IPMK elicited a 50% decrease in Paneth cell number (Figure 4D). Higher magnification confocal imaging of Paneth cell marker Lysozyme (Figures 4E–4G) and Periodic acid-Schiff (PAS)/alcian-blue-staining (Figure S4F) of intestinal sections of *Ipmk^{ΔIEC}* mice, revealed pronounced abnormalities in Paneth cells, including aberrant, disorganized granules, as well as decreased numbers of granules (Figures 4E–4G and S4F). Histological analysis of these sections from four controls and four mutant mice revealed a 100% concordance between *Ipmk* genotype and abnormal Paneth cell morphology.

Paneth cell disorganization is known to contribute to Crohn disease pathology.²³ GWAS data⁷ revealed a significant association between IPMK variants and risk for IBD. Four SNPs at the IPMK locus were significantly associated with IBD. SNPs that have statistically significant associations with Crohn disease include rs1819658, located in an enhancer of the IPMK gene (p = 9.0 × 10⁻¹⁷), and rs2790216, located in intron 1 of

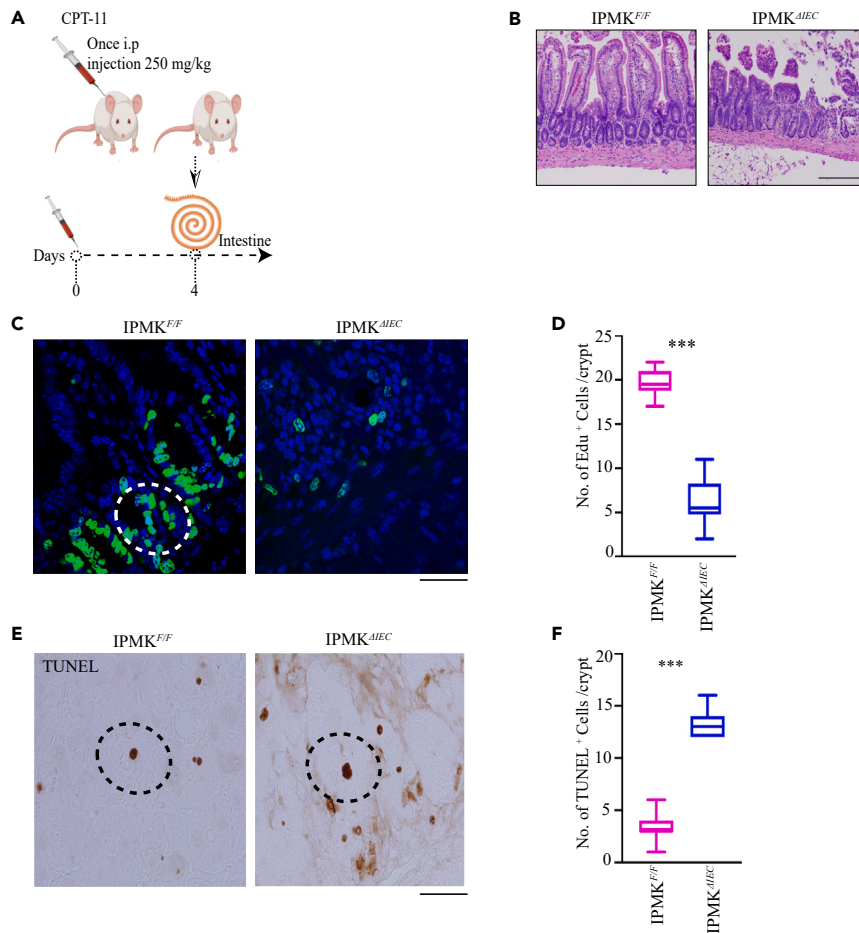


Figure 5. IPMK enhances intestinal epithelial repair

- (A) Schematic of CPT-11 treatment plan.
- (B) H&E staining of CPT-11-treated ileum sections from *Ipmk*^{ΔIEC} and *Ipmk*^{F/F} mice. Scale bar 200 μm.
- (C) EdU (green) and DAPI (blue) staining 2h after injection in CPT-11-treated intestines. Scale bar 20 μm (white circle specifies Edu positive cell).
- (D) Quantitation of EdU-positive cells. n = 4 mice each group, ***p < 0.001. Data are graphed as mean ± SD.
- (E and F) TUNEL-positive cells (dark brown and black dotted circle) after CPT-11 treatment in *Ipmk*^{F/F} and *Ipmk*^{ΔIEC} ileum. Scale bar 20 μm, (F) Quantitation of TUNEL-positive cells. n = 4 mice each group, ***p < 0.001. Data are graphed as mean ± SD.

IPMK (p = 8.0 × 10⁻⁹) (Figure S4G). Two additional SNPs were also associated with IBD (not presented in Figure S4G): rs2153283, located in intron 4 of *IPMK* (IBD p = 2 × 10⁻¹¹, MAF: 0.40, alleles C/A), and rs1199103, an intergenic variant (IBD, p = 5 × 10⁻¹¹, MAF: 0.40, alleles A/C/G).

Epithelial cells are born at the base of the intestinal crypts and migrate to the tip of the villus, where they reside until they die (Figure S4H). A recent study showed that active cell migration is critical for maintaining intestinal homeostasis.²³ We examined the influence of IPMK on IEC migration 48 h after injection of EdU. Intestinal deletion of IPMK strikingly impeded IEC migration from the crypt to the villus tip (Figure S4H). In summary, loss of IPMK expression in IECs led to impaired epithelial cell proliferation, Paneth cell abnormalities, and diminution of IEC migration to the villus tip.

Inositol polyphosphate multikinase enhances intestinal epithelial repair

AKT promotes IEC proliferation during damage-induced intestinal tissue repair.²² To investigate a potential role for IPMK in recovery from chemotherapy-induced acute intestinal injury, we treated *Ipmk*^{F/F} and *Ipmk*^{ΔIEC} mice with a single dose of CPT-11 (irinotecan) (250 mg/kg), an agent currently being explored as a treatment

for colorectal cancer (Figure 5A) and analyzed intestinal tissue 4 days later. Histopathological analysis revealed the regeneration of crypts and epithelial layers in *lpmk^{F/F}* mice. By contrast, *lpmk^{ΔIEC}* mice displayed significant impairment in the healing of crypts (Figure 5B). We found extensive depletion of EdU-positive cells in *lpmk^{ΔIEC}* mice relative to *lpmk^{F/F}* mice, indicating that IPMK is a mediator of intestinal regeneration (Figures 5C and 5D). Loss of regeneration in *lpmk^{ΔIEC}* mice was associated with a pronounced increase in apoptosis, as evident from TUNEL staining (Figures 5E and 5F). Taken together, these data demonstrate that IPMK plays a critical role in regenerative responses to intestinal toxins.

DISCUSSION

We previously established IPMK as a novel mammalian PI3k.³ Recently, Jung et al. showed loss of AKT activation in IPMK-depleted primary hepatocytes.²⁴ However, the physiological implications of IPMK's PI3k activity have remained obscure. Here we show that the PI3k activity of IPMK is critical for PDK1 membrane localization, which promotes the activation of AKT and ROCK1 to stimulate intestinal epithelial cell migration, proliferation, and regeneration.

It is well accepted that cPI3k generates PIP₃ at the plasma membrane, an action required for AKT membrane localization and PDK1- and mTORC2-mediated AKT phosphorylation. We found that the deletion of IPMK abolished AKT phosphorylation at both Thr308 and Ser473 by around 60% (Figures 1D–1F, S1D, and S1E), a deficit which could be rescued by WT IPMK, but not by an IPMK mutant lacking kinase activity (Figure 3H). However, the PI3k activity of cPI3k (p110 α , β , γ , and δ) remained intact after IPMK deletion (Figure S1C). Accordingly, we explored mechanisms of IPMK-mediated AKT activation. Confocal imaging and cell fractionation studies demonstrated that AKT membrane localization was independent of IPMK and mediated by cPI3k (Figures 2C–2E). Previously, we showed⁵ that the deletion of IPMK impaired mTORC2 activation and thus diminished AKT Ser473 phosphorylation (Figures S1D and S1E). We wondered whether IPMK-derived PIP₃ controls the kinases that phosphorylate AKT. PDK1 is the first discovered AKT kinase and, like AKT itself, is recruited to the membrane by PIP₃.¹⁶ The cPI3ki wortmannin²² fails to inhibit PDK1 membrane localization.¹⁰ Similarly, Pinner et al.¹² found that PIP₃-mediated PDK1 membrane localization helps to dissociate ROCK1 from inhibitory RhoE binding, thus promoting cell migration; this action was likewise mostly unaffected by cPI3ki.¹² We also showed that a cPI3ki had no effect on the PI3k activity of IPMK.³ Here we found that the PI3k activity of IPMK is critical for PDK1 membrane localization, which was minimally influenced by the cPI3ki pictilisib (Figures 3B–3F). Deletion of IPMK also impaired PDK1-mediated ROCK1 activation by preventing the dissociation of ROCK1 from RhoE (Figures S3C and S3D) and diminished cell migration (Figure S3E), which is in agreement with the previous study by Sekine et al.²⁵ However, the recruitment of PDK1 to the membrane does not require physical interaction between PDK1 and IPMK (data not shown). This finding establishes IPMK as a critical mammalian PI3k that promotes the membrane localization of PDK1, one of the principal kinases that triggers AKT activation. In contrast to conventional wisdom, PDK1 membrane localization is mostly independent of cPI3k.

Activation of AKT is essential for maintaining the homeostasis of regenerative organs.²⁴ The intestine is a highly regenerative organ, and the loss of AKT function in the intestine impairs intestinal epithelial cell regeneration.²² Activation of AKT is critical for maintaining homeostasis of the Paneth cell, a specialized intestinal cell type that resides in ileal crypts and secretes antibacterial peptides and growth factors to regulate intestinal bacterial flora and nurture intestinal stem cells. Intestinal deletion of IPMK markedly reduced PDK1-mediated AKT Thr308 phosphorylation (Figure 4B) and IEC proliferation both under basal conditions and during recovery from chemotherapy-induced tissue damage (Figures 4C and 5). *lpmk^{ΔIEC}* mice showed a striking loss of Paneth cell number accompanied by pronounced abnormalities in the organization of Paneth cell granules (Figures 4D–4G). This Paneth cell abnormality has been observed in Crohn disease.²⁶ Genome-wide association studies previously identified IPMK as a major Crohn's disease-related gene (Figure S4G). Thus, loss of function of IPMK may drive pathology in Crohn disease and IBD by impairing AKT-mediated Paneth cell integrity. Detailed analysis of how IPMK influences Paneth cell biology and maintenance of ISC (intestinal stem cell) will be done in future studies creating Paneth cell-specific and ISC-specific IPMK KO mice lines.

In summary, IPMK is a novel PI3k for PDK1 that activates AKT and promotes ROCK1-mediated cell migration. PDK1 membrane localization and PDK1-dependent AKT phosphorylation are critically regulated by the PI3k activity of IPMK and are independent of cPI3k. By contrast, the PI3k activity of IPMK is dispensable for AKT membrane localization, which depends exclusively on cPI3k (Figure 6A). IPMK-mediated AKT

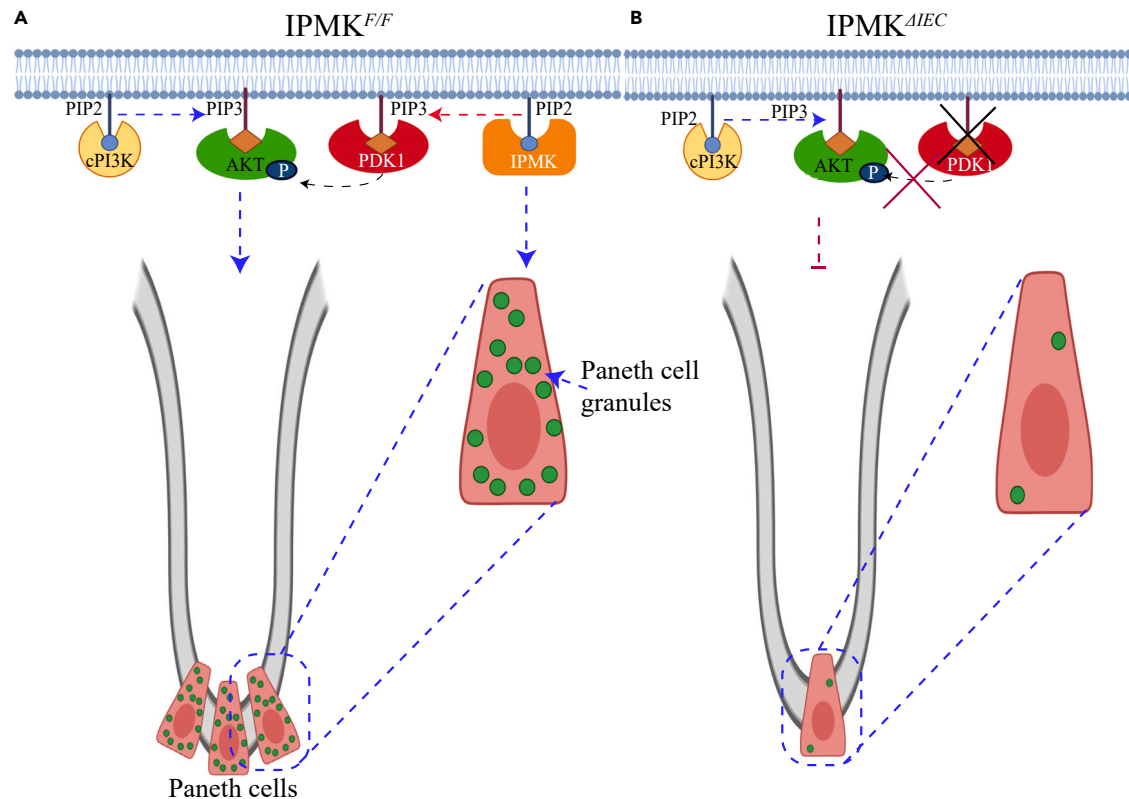


Figure 6. Schematic diagram depicting the role of IPMK in PDK1-mediated AKT activation and intestinal homeostasis

(A) Under normal conditions, IPMK promotes PDK1 membrane localization and PDK1-dependent AKT phosphorylation. The PI3k activity of IPMK is, however, expendable for AKT membrane localization, which exclusively depends on cPI3k. PDK1-dependent activation of AKT maintains Paneth cell homeostasis. (B) Deletion of IPMK (*Ipmk^{ΔIEC}*) impairs PDK1 membrane localization and PDK1-dependent AKT phosphorylation, rendering AKT inactive. Loss of function of AKT impairs intestinal proliferation and Paneth cell function in the crypt (e.g., loss of Paneth cell number and dysregulation of intracellular granules).

activation promotes intestinal regeneration by maintaining Paneth cell homeostasis. Differences in IPMK activity may contribute to the risk for Crohn disease, and drugs targeting the PI3k activity of IPMK may have potential as novel treatments for Crohn disease and related conditions.

Limitations of the study

Intestinal regeneration is directly linked to several intestinal diseases. Crosstalks of different cell types with intestinal stem cells determine the fate of intestinal regeneration. Our research, for the first time, shows the importance of IPMK in ileum health. In our study, the observations of loss of Paneth cells in IPMK-deleted intestine indicates that IPMK is critical for intestinal regeneration and may be linked to Crohn disease. While our study has uncovered roles of IPMK in intestinal regeneration, it is predominantly observational and missing a direct link with intestinal stem cells. Future work will help understand the link between IPMK/intestinal stem cell and regeneration.

STAR★METHODS

Detailed methods are provided in the online version of this paper and include the following:

- KEY RESOURCES TABLE
- RESOURCE AVAILABILITY
 - Lead contact
 - Materials availability
 - Data and code availability
- EXPERIMENTAL MODEL AND SUBJECT DETAILS
 - Animals

- Generation of intestine-specific IPMK KO mice
- Cell culture
- Plasmids and transfection
- Retroviral transfection and generation of stably transfected cells
- Transient transfection
- AKT activation in cell culture
- Cytoplasm and cell membrane isolation
- Immunoprecipitation
- *In vitro* AKT and PDK1 kinase activity assay
- AKT and PDK1 membrane localization
- Western Blot
- Wnt 3A treatment and protein expression
- Immunohistochemistry, immunofluorescence and DAB stain
- TUNEL staining
- Periodic acid Schiff staining
- EdU treatment and tissue regeneration study
- Intestinal and MEF cell migration
- CPT-11 treatment and tissue repair study
- Enteroid isolation from IPMK wild type and conditional knockout mice
- Confocal microscopy
- **QUANTIFICATION AND STATISTICAL ANALYSIS**

SUPPLEMENTAL INFORMATION

Supplemental information can be found online at <https://doi.org/10.1016/j.isci.2023.106623>.

ACKNOWLEDGMENTS

We sincerely thank Dr. Gregg Semenza for his critical comments to shape the article. We are thankful to Dr. Jingchun Chen for her help in sharing instruments. This work was supported by National Institute of Health, United States, grant 5R01MH018501-48, 5P20GM121325-5854, 5P20GM121325-8158, and P20GM121325. We like to thank NIPM core for assisting with instruments and experiments.

AUTHOR CONTRIBUTIONS

PG conceived and designed the experiments. PG, LR, ERS, EA, GK, SC, and YS performed the experiments. SHM analyzed the data involving IPMK's contribution to the cellular PIP₃ pool, and SHM and PM performed the analysis of intestinal cell migration. PG, SAW, MD, and SHS analyzed the data. PG, ERS, and SM edited the article. PG and SHS wrote the article.

DECLARATION OF INTERESTS

The authors declare no competing interests.

Received: June 5, 2022

Revised: February 22, 2023

Accepted: April 3, 2023

Published: April 11, 2023

REFERENCES

1. Berridge, M.J., Lipp, P., and Bootman, M.D. (2000). The versatility and universality of calcium signalling. *Nat. Rev. Mol. Cell Biol.* *1*, 11–21. <https://doi.org/10.1038/35036035>.
2. Saiardi, A., Erdjument-Bromage, H., Snowman, A.M., Tempst, P., and Snyder, S.H. (1999). Synthesis of diphosphoinositol pentakisphosphate by a newly identified family of higher inositol polyphosphate kinases. *Curr. Biol.* *9*, 1323–1326.
3. Maag, D., Maxwell, M.J., Hardesty, D.A., Boucher, K.L., Choudhari, N., Hanno, A.G., Ma, J.F., Snowman, A.S., Pietropaoli, J.W., Xu, R., et al. (2011). Inositol polyphosphate multikinase is a physiologic PI3k that activates akt/PKB. *Proc. Natl. Acad. Sci. USA* *108*, 1391–1396. <https://doi.org/10.1073/pnas.1017831108>.
4. Guha, P., Tyagi, R., Chowdhury, S., Reilly, L., Fu, C., Xu, R., Resnick, A.C., and Snyder, S.H. (2019). IPMK mediates activation of ULK signaling and transcriptional regulation of autophagy linked to liver inflammation and regeneration. *Cell Rep.* *26*, 2692–2703.e7. [S2211-1247\(19\)30175-5 \[pii\]](https://doi.org/10.1016/j.celrep.2019.03.017).
5. Kim, S., Kim, S.F., Maag, D., Maxwell, M.J., Resnick, A.C., Juluri, K.R., Chakraborty, A., Koldobskiy, M.A., Cha, S.H., Barrow, R., et al. (2011). Amino acid signaling to mTOR mediated by inositol polyphosphate multikinase. *Cell Metabol.* *13*, 215–221. <https://doi.org/10.1016/j.cmet.2011.01.007>.

6. Sei, Y., Zhao, X., Forbes, J., Szymczak, S., Li, Q., Trivedi, A., Voellinger, M., Joy, G., Feng, J., Whatley, M., et al. (2015). A hereditary form of small intestinal carcinoid associated with a germline mutation in inositol polyphosphate multikinase. *Gastroenterology* 149, 67–78. <https://doi.org/10.1053/j.gastro.2015.04.008>.
7. Yokoyama, J.S., Wang, Y., Schork, A.J., Thompson, W.K., Karch, C.M., Cruchaga, C., McEvoy, L.K., Witoelar, A., Chen, C.H., Holland, D., et al. (2016). Association between genetic traits for immune-mediated diseases and alzheimer disease. *JAMA Neurol.* 73, 691–697. <https://doi.org/10.1001/jamaneurol.2016.0150>.
8. Hoxhaj, G., and Manning, B.D. (2020). The PI3K-AKT network at the interface of oncogenic signalling and cancer metabolism. *Nat. Rev. Cancer* 20, 74–88. <https://doi.org/10.1038/s41568-019-0216-7>.
9. Sarbassov, D.D., Guertin, D.A., Ali, S.M., and Sabatini, D.M. (2005). Phosphorylation and regulation of akt/PKB by the rictor-mTOR complex. *Science* 307, 1098–1101.
10. Komander, D., Fairservice, A., Deak, M., Kular, G.S., Prescott, A.R., Peter Downes, C., Safrany, S.T., Alessi, D.R., and van Aalten, D.M.F. (2004). Structural insights into the regulation of PDK1 by phosphoinositides and inositol phosphates. *EMBO J.* 23, 3918–3928. <https://doi.org/10.1038/sj.emboj.7600379>.
11. Ebner, M., Sinkovics, B., Szczygieł, M., Ribeiro, D.W., and Yudushkin, I. (2017). Localization of mTORC2 activity inside cells. *J. Cell Biol.* 216, 343–353. <https://doi.org/10.1083/jcb.201610060>.
12. Pinner, S., and Sahai, E. (2008). PDK1 regulates cancer cell motility by antagonising inhibition of ROCK1 by RhoE. *Nat. Cell Biol.* 10, 127–137. <https://doi.org/10.1038/ncb1675>.
13. Gagliardi, P.A., di Blasio, L., Puliafito, A., Seano, G., Sessa, R., Chianale, F., Leung, T., Bussolino, F., and Primo, L. (2014). PDK1-mediated activation of MRCKalpha regulates directional cell migration and lamellipodia retraction. *J. Cell Biol.* 206, 415–434. <https://doi.org/10.1083/jcb.201312090>.
14. Resnick, A.C., Snowman, A.M., Kang, B.N., Hurt, K.J., Snyder, S.H., and Saiardi, A. (2005). Inositol polyphosphate multikinase is a nuclear PI3k with transcriptional regulatory activity. *Proc. Natl. Acad. Sci. USA* 102, 12783–12788. 0506184102 [pii].
15. Sarkaria, J.N., Tibbetts, R.S., Busby, E.C., Kennedy, A.P., Hill, D.E., and Abraham, R.T. (1998). Inhibition of phosphoinositide 3-kinase related kinases by the radiosensitizing agent wortmannin. *Cancer Res.* 58, 4375–4382.
16. Franke, T.F. (2008). PI3K/akt: Getting it right matters. *Oncogene* 27, 6473–6488. <https://doi.org/10.1038/onc.2008.313>.
17. Jacinto, E., Facchinetti, V., Liu, D., Soto, N., Wei, S., Jung, S.Y., Huang, Q., Qin, J., and Su, B. (2006). SIN1/MIP1 maintains rictor-mTOR complex integrity and regulates akt phosphorylation and substrate specificity. *Cell* 127, 125–137.
18. Casamayor, A., Morrice, N.A., and Alessi, D.R. (1999). Phosphorylation of ser-241 is essential for the activity of 3-phosphoinositide-dependent protein kinase-1: Identification of five sites of phosphorylation in vivo. *Biochem. J.* 342, 287–292.
19. Sheng, H., Shao, J., Townsend, C.M., and Evers, B.M. (2003). Phosphatidylinositol 3-kinase mediates proliferative signals in intestinal epithelial cells. *Gut* 52, 1472–1478. <https://doi.org/10.1136/gut.52.10.1472>.
20. He, X.C., Yin, T., Grindley, J.C., Tian, Q., Sato, T., Tao, W.A., Dirisina, R., Porter-Westpfahl, K.S., Hembree, M., Johnson, T., et al. (2007). PTEN-deficient intestinal stem cells initiate intestinal polyposis. *Nat. Genet.* 39, 189–198.
21. Harnack, C., Berger, H., Antanaviciute, A., Vidal, R., Sauer, S., Simmons, A., Meyer, T.F., and Sigal, M. (2019). R-spondin 3 promotes stem cell recovery and epithelial regeneration in the colon. *Nat. Commun.* 10, 4368. Article number: 4368. <https://doi.org/10.1038/s41467-019-12349-5>.
22. Goldsmith, J.R., Spitofsky, N., Zamani, A., Hood, R., Boggs, A., Li, X., Li, M., Reiner, E., Ayyaz, A., Etwebi, Z., et al. (2020). TNFAIP8 controls murine intestinal stem cell homeostasis and regeneration by regulating microbiome-induced akt signaling. *Nat. Commun.* 11, 2591–2592. <https://doi.org/10.1038/s41467-020-16379-2>.
23. Thachil, E., Hugot, J.P., Arbeille, B., Paris, R., Grodet, A., Peuchmaur, M., Codogno, P., Barreau, F., Ogier-Denis, E., Berrebi, D., and Viala, J. (2012). Abnormal activation of autophagy-induced crinophagy in paneth cells from patients with crohn’s disease. *Gastroenterology* 142, 1097–1099.e4. <https://doi.org/10.1126/science.aau3429>.
24. Jung, I.R., Anokye-Danso, F., Jin, S., Ahima, R.S., and Kim, S.F. (2022). IPMK modulates hepatic glucose production and insulin signaling. *J. Cell. Physiol.* 237, 3421–3432. <https://doi.org/10.1002/jcp.30827>. Epub 2022 Jul 13.
25. Tu-Sekine, B., Padhi, A., Jin, S., Kalyan, S., Singh, K., Apperson, M., Kapania, R., Hur, S.C., Nain, A., and Kim, S.F. (2019). Inositol polyphosphate multikinase is a metformin target that regulates cell migration. *FASEB J.*, Dec 33, 14137–14146. <https://doi.org/10.1096/fj.201900717RR>.
26. Cadwell, K., Liu, J.Y., Brown, S.L., Miyoshi, H., Loh, J., Lennerz, J.K., Kishi, C., Kc, W., Carrero, J.A., Hunt, S., et al. (2008). A key role for autophagy and the autophagy gene Atg16l1 in mouse and human intestinal paneth cells. *Nature* 456, 259–263. <https://doi.org/10.1038/nature07416>.

STAR★METHODS

KEY RESOURCES TABLE

REAGENT or RESOURCE	SOURCE	IDENTIFIER
Antibodies		
β-Actin	Cell Signaling	4967;RRID: AB_330288
phospho-myosin light chain 2 (Thr18/Ser19)	Cell Signaling	3674
RhoE	Cell Signaling	3664
phospho-AKT (Ser473)	Cell Signaling	4060
phospho-AKT (Thr308)	Gene Tex Cell Signaling	GTX79150 9275
Lysozyme	Ab Cam	108508
Phospho-β-catenin-S552	ABclonal	AP0579
Myosin Light Chain 2 antibody	Proteintech	AP0579
ROCK1	Bethyl Laboratories	A300-457A
Goat anti-Rabbit, Alexa Fluor 488 antibody	Invitrogen	A-11008
GSK2α Ser 21	Cell Signaling	9331
HRP-Anti Mouse	GE Health care	NA931V
IgG control antibody	Cell signaling	2729
Mouse specific Anti-IPMK	Lab generated	NA
HRP-Anti Rabbit	GE Health care	GENA934
GFP	Cell Signaling	2555
Myc	Cell Signaling	2276
Biological samples		
AKT-PH-GFP	Addgene	51465
GFP-PDK1	Addgene	134189
pMX-myc	Snyder Lab	NA
pMX-wIPMK	Snyder Lab	NA
pMX-IPMK-KSA	Snyder Lab	NA
Chemicals, peptides and recombinant proteins		
Pictilisib GDC-0941	Millipore Sigma	957054-30-7
LY294002	Selleckchem	S1105
Ezview myc Beads	Sigma	E6654
PVDF membrane	Millipore Sigma	IPVH00010
DMEM (w/o glucose)	Thermo Fischer Scientific	25030081
FBS	Thermo Fischer Scientific	F2442
DMEM	Thermo Fischer Scientific	11960-0; 512449655
L-glutamine	Thermo Fischer Scientific	25030081
Lipofectamine 3000	Thermo Fischer Scientific	L3000015
Paraformaldehyde 4% solution in PBS	Thermo Fischer Scientific	J19943.K2
Hydrogen peroxide	Thermo Fischer Scientific	202465000
Penicillin/streptomycin	Thermo Fischer Scientific	15140122
DMSO Cell culture grade	Thermo Fischer Scientific	J66650.AP
Irinotecan hydrochloride (CPT-11)	Sigma	I1406-50mg
ImmPACT® DAB Peroxidase (HRP) Substrate	Vector Biolab	SK-4105
DyLight 594 Streptavidin	Vector Biolab	SA-5594
Antigen Retrieval Reagent-Universal	R&D systems	CTS015

(Continued on next page)

Continued

REAGENT or RESOURCE	SOURCE	IDENTIFIER
EZview™ Red Protein G Affinity Gel	Sigma-Aldrich	E3403-1ml
Click-iT™ EdU Cell Proliferation Kit for Imaging, Alexa Fluor™ 488	ThermoFisher	C10337
VECTASHIELD® Antifade Mounting Medium	Vector Biolab	H-1000-10
2.5% Normal Goat Serum Blocking Solution	Vector Biolab	S-1012-50
Citrate Buffer pH 6.0	Sigma Aldrich	C9999-100ml
Polybrene	Tocris	7711
Blasticidin	Thermo Scientific	A1113903
HEPES	Sigma Life science	H0887
Potassium acetate	Thermo Scientific	AM9610
MgCl2	Thermo Scientific	012315.C4
Recombinant AKT1/PKB1 protein	Millipore Sigma	14-279
Super Signal™ West Femto Luminol	Thermo Scientific	1859022
Recombinant Wnt 3A	R&D system	5036-WN
Histo-Clear	Fisher Scientific	5089990147
6-diamidino-2-phenylindole	Thermo Fisher Scientific	D1306
IntestiCult™ Enteroid Growth Medium	STEM CELL Technologies	06005
Gentle Cell Dissociation Reagent	STEM CELL Technologies	100-0485

Critical commercial assays

PIP_3 mass ELISA kit	Echelon Biosciences	K-2500S
ProteoExtract® Subcellular Proteome Extraction Kit	Millipore-Sigma	539790
TumorTACS™ <i>In Situ</i> Apoptosis Detection Kit	R&D Systems	4815-30-K
Periodic Acid Schiff Stain Kit	Abcam	Ab150680

Experimental models: Cell lines

Mouse Embryonic fibroblast	Snyder Lab	NA
Human Embryonic Kidney Cell	ATCC	ATCC-CRL-1932

Experimental models: Organisms/strains

IPMK F/F mice 129SV-C57 BL/6 mixed background	Ozgene	Custom Developed
Albumin Cre mice c57BL/6J <i>lpmk^{dIEC}</i>	Jackson laboratory	3574
	Ozgene	Custom Developer

Software and algorithms

ZEN lite	Carl Zeiss	https://www.zeiss.com/microscopy/int/downloads.html?vaURL=www.zeiss.com/microscopy/int/downloads/zen.html
ImageJ	NIH ImageJ	https://imagej.nih.gov/ij/
Graph Pad prism 8	Graph Pad prism	https://www.graphpad.com/scientific-software/prism/
Illustrator CC	Adobe	https://www.adobe.com/products/illustrator/free-trial-download.html
ImageXpress Micro XLS widefield high-content analysis system	Molecular devices	https://www.moleculardevices.com/products/cellular-imaging-systems?
ImarisX64	OXFORD instruments	https://imaris.oxinst.com/products/imaris-for-cell-biologists?gclid=CjwKCAiAjPyfBhBMEiwAB2CCIt-pe1x8x9GzTbItQo2bRnx74Tdycz-zEQD5DxMwi6zZbmcvOZv6RoCwglQAvD_BwE

RESOURCE AVAILABILITY

Lead contact

Further information and requests for resources and reagents should be fulfilled by the Lead Contact, Dr. Prasun Guha, Ph.D. (prasun.guha@unlv.edu).

Materials availability

Plasmids and mouse lines generated in this study are available from the [lead contact](#) upon reasonable request with a completed Materials Transfer Agreement.

Data and code availability

- This paper does not report the original code.
- This paper does not have any genomic or sequencing data.
- Any additional information required to reanalyze the data reported in this paper is available from the [lead contact](#) upon request.

EXPERIMENTAL MODEL AND SUBJECT DETAILS

Animals

All protocols were approved by the Johns Hopkins University Animal Care and Use Committee. Mice were housed according to institutional guidelines, in a controlled environment at a temperature of $22^{\circ}\text{C} \pm 1^{\circ}\text{C}$, under a 12-h dark-light period and provided with standard chow diet and water *ad libitum*. Male and female IPMK F/F, IPMK F/F-Alb Cre, (between 1 and 3-month-old) were used. Specifically, male mice were used for liver regeneration study, electron microscopy and tissue histology. All mice were maintained in 129SV-C57BL/6 mixed background.

Generation of intestine-specific IPMK KO mice

Ipmk^{F/F} mice were generated as previously described (22). *Ipmk*^{F/F} mice were crossed with C57BL/6J mice carrying Cre expressed under the control of the murine villin promoter as described previously (34) to create intestinal-specific *Ipmk* knockout mice (*Ipmk*^{ΔIEC}). Homozygous *Ipmk*^{F/F} mice were crossed with the *Ipmk*^{ΔIEC} mice, which mediate excision of floxed alleles in the intestine. All mice were maintained on a C57BL/6J background and were 7th generation backcrossed. C57BL/6J mice were used for Enteroid isolation for inhibitor treatment as well as for DSS and CPT-11 treatments. Mice were housed in a 12-hour light/12-hour dark cycle at 22°C and fed standard rodent chow. All research involving mice was approved by the Johns Hopkins Animal Care and Use Committee.

Cell culture

Mouse embryonic fibroblast (MEF) and human embryonic kidney (HEK) cells were cultured in Dulbecco's modified Eagles medium (DMEM) supplemented with 10% FBS, 2 mM L-glutamine, 100 U/mL penicillin, and 100 mg/mL streptomycin. IPMK WT and KO MEF cells were developed in our lab as previously described,³ briefly, floxed MEFs were immortalized by transfection with pSG5- Large T (deposited by William Hahn to Addgene) using Polyfect transfection reagent (Qiagen) according to the manufacturer's protocol. After serial-passaging transfected cells five times to select against nontransformed cells, IPMK KO cells were generated by transduction of floxed cells with adenovirus carrying the gene encoding the Cre recombinase (University of Iowa Gene Transfer Vector Core). The virus was combined with GeneJammer (Stratagene) transfection reagent to enhance transduction efficiency. After transduction, clonal populations were colony purified and screened for IPMK expression.³

Plasmids and transfection

AKT-PH-GFP and GFP-PDK1 plasmids were from Addgene. pMX-myc, pMX-wIPMK and pMX-IPMK-KSA were generated in-lab.

Retroviral transfection and generation of stably transfected cells

Target vector DNA retroviral constructs were transiently transfected into a Platinum-E (Plat-E) retrovirus packaging cell line for 48 hours by using Lipofectamine 3000 transfection reagent. High-titer viral stocks were harvested by passing the supernatant through a 0.45 μm filter. For infection, MEFs were incubated

with the viral supernatant in the presence of polybrene (8 µg/mL) for 48 hours. Stably infected MEFs were selected by treatment with blasticidin (4 µg/mL) for 1-2 weeks. Selected stable cell lines were continuously maintained in medium containing blasticidin (4 µg/mL).

Transient transfection

MEF cells were transfected with Lipofectamine 3000 (ThermoFisher) per manufacturer protocol.

AKT activation in cell culture

To evaluate AKT phosphorylation in MEF cells, 5×10^6 cells were seeded in 10 cm plates and left to attach to the plate for 3 hours. Cells were then washed with room temperature phosphate-buffered saline (PBS) followed by incubation of cells in serum-free DMEM supplemented with 2 mM L-glutamine, 100 U/mL penicillin, and 100 mg/mL streptomycin. After 24 hours of serum starvation, serum-free media was replaced with complete DMEM (10% FBS) for 5 minutes to promote AKT membrane localization. Cells given the cPI3ki GDC0941/pictilisib were pretreated for 30 minutes prior to complete DMEM administration with GDC0941 (100 nM) in serum-free media. After 5 minutes of serum stimulation, cells were quenched with cold PBS and lysed as previously described.

Cytoplasm and cell membrane isolation

Cytoplasm and membrane fractions were obtained using the ProteoExtract® Subcellular Proteome Extraction Kit (Millipore-Sigma) following manufacturer protocol.

Immunoprecipitation

Immunoprecipitation of endogenous ROCK-I was performed with 1 mg of protein lysates in lysis buffer (150mM NaCl, 0.5% CHAPS, 0.1% Triton, 0.1% BSA, 1mM EDTA, protease inhibitors, and phosphatase inhibitors). Protein lysate was incubated for 2 hrs. at 4°C with ROCK1 antibody (Bethyl) followed by EZview Protein G beads (Sigma) for 1 h. Beads were pelleted at 1000xg and washed with lysis buffer 3 times for 5 minutes each on a rocking platform at 4°C, and SDS sample buffer loading dye was added. Immunoprecipitated samples were resolved by polyacrylamide gel electrophoresis and binding of RhoE was observed by Western blot.

In vitro AKT and PDK1 kinase activity assay

To perform *In vitro* PDK1 kinase assay 3 µg of PDK1/ AKT antibody was added to 1.5 mg of lysates and incubated with rotation for 2 hours at 4°C. 15 µL of protein G beads was added and the incubation continued for an additional hour. PDK1/AKT immunoprecipitates were washed four times with the same lysis buffer and twice with the kinase buffer (25 mM HEPES [pH 7.5], 100 mM potassium acetate, 1 mM MgCl₂). Kinase assays were performed for 20 min at 37 °C in a final volume of 15 microliters of kinase buffer containing 500 µM ATP and 500 ng inactive AKT1/PKB1 (Millipore) as a substrate for PDK1 and GSK3 α for AKT. Reaction was stopped by resuspending beads in SDS-containing sample buffer and boiling samples for 5 minutes followed by western blot of phosphor-AKT Thr308 and GSK3 α Ser 21.

AKT and PDK1 membrane localization

5×10^5 MEF cells were seeded on 35 mm glass-bottom cell culture dishes and left to proliferate for 3 hours. Cells were then transfected with 500 ng AKT-PH-GFP using Lipofectamine 3000 following manufacturer's recommendations. 24 hours after transfection, cells were washed with PBS and deprived of serum by exchanging complete DMEM with FBS-free media as previously described. After 24 hours of serum starvation, serum-free media was replaced with complete DMEM (10% FBS). Cells given the cPI3ki GDC0941/pictilisib were treated as described above. After 5 minutes of serum stimulation, cells were quenched with cold PBS and fixed using chilled 4% paraformaldehyde. Cells were stained with DAPI (1 µg/mL) in PBS. After staining, coverslips were mounted with antifade (Vectashield) mounting media. Cells were imaged via confocal microscopy; images were exported as .czi files to ImageJ (NIH). For each image, well-defined and intact portions of the membrane were traced using the "segmented line" function with spline-fit, setting the line thickness such that the selection covered 2.5 µm across the membrane. This was followed by transformation using the "straighten" function to generate a uniform, straight section of membrane. This image was rotated such that the left of the image was the intracellular space and the right side was the extracellular space, with the edge of the membrane lying in the middle of the image. A plot profile was generated using this image, yielding a trace of the gray value across the membrane, progressing

intra- to extracellular down the x-axis. The data produced by this plot was exported to Excel. As the transfection efficiency differed slightly between cells, data from each image was normalized from 0 to 1, with 0 being the extracellular space and 1 being the maximum gray value. Using this data, the difference between cytoplasm and membrane fluorescence was calculated.

Western Blot

Cell lysates were first prepared using lysis buffer (50mM Tris-HCl, 150mM NaCl, 1mM EDTA, 1% Triton X-100 in PBS, phosphatase inhibitors, protease inhibitors). Samples were centrifuged at 16,200xg for 10 min, followed by total protein quantification. Proteins were resolved by SDS-polyacrylamide gel electrophoresis and transferred to PVDF membranes. Membranes were incubated in 1:1000 dilution of primary antibody in 20 mM Tris-HCl (pH 7.4), 150 mM NaCl, and 0.02% Tween 20 (Tris-buffered saline/Tween 20, TBST) with 3% BSA overnight at 4°C on a rocking platform. The membranes were washed 3 times with Tris-buffered saline/Tween-20, then incubated with HRP-conjugated secondary antibody (GE Health Care) diluted 1:5000 in TBST with 3% BSA, and the bands visualized by chemiluminescence (ThermoFisher). The blots shown in the figures were representative replicates selected from at least 3 experiments. Densitometric analysis was performed using ImageJ software.

Wnt 3A treatment and protein expression

Recombinant Wnt 3A (R&D system) was diluted in water. Cells were treated with 250 ng/ml of Wnt 3A diluted in serum-free medium and incubated for 24h.

Immunohistochemistry, immunofluorescence and DAB stain

Mice were sacrificed via CO₂. Immediately following euthanasia, the intestine was removed and flushed with cold PBS. The intestine was subsequently opened lengthwise and washed in cold PBS, then cut into approximately 3-4 mm fragments for sectioning and paraffinization. Samples were deparaffinized with Histo-Clear (Thermo Fisher) and rehydrated in successive washes of 100%, 90%, and 75% ethanol followed by deionized (DI) water. Sections were unmasked via heat-induced epitope retrieval (HIER) using citrate buffer, followed by blocking with 2.5% goat serum for 1 hour. Primary antibodies were diluted per manufacturer's recommendation in Triton-X diluted to 1% in PBS, incubating overnight at 4°C in a humidified chamber. The following day, samples were washed with TBST, followed by incubation with fluorescent-tagged secondary antibodies diluted in 1% Triton-X solution for 60 minutes. After washing with TBST, samples were stained with 4', 6-diamidino-2-phenylindole (DAPI) diluted in PBS (1 µg/mL). Slides were imaged using a slide scanner and confocal microscopy.

To identify the influence of IPMK deletion on Paneth cell, we used lysozyme to detect Paneth cells. These, along with anti-Beta-catenin Ser 522, anti-IPMK, and IgG control antibodies, were all anti-rabbit and targeted with fluorescent secondary Alexa Fluor488. Additionally, F4/80 staining (used to detect inflammatory cells) was detected using Alexa Fluor 488-tagged anti-mouse secondary antibodies. Phospho-AKT Thr308 antibodies were targeted with Alexa Fluor488-tagged anti-rabbit antibodies.

Tissue samples of the small intestine, large intestine, lung, kidney, liver, skeletal muscle, cardiac muscle, pancreas, skin, and lymph were sectioned and paraffinized as described above. Endogenous peroxidase activity was first blocked with [0.1%] H₂O₂ for 5 minutes. Sections were incubated with IPMK antibody followed by HRP-tagged secondary antibody, then treated with diaminobenzidine (DAB) substrate. Sections were counterstained with hematoxylin. Images were acquired at 40x magnification with an Olympus microscope. Hematoxylin and DAB channels were separated using the ImageJ color deconvolution macro, which utilizes an RGB image deconvolution method developed by Ruifrok and Johnston (36). Subsequent histogram analysis in ImageJ produced signal intensities from 0-255, with 0 = darkest intensity (positive staining) and 255 representing a white, unstained signal. A threshold of 0-230 was applied to eliminate background staining; using this threshold, the MGV of the tissue samples was determined. Using the MGV, the optical density (OD) of each piece was determined using the equation $OD = \log_{10} \frac{I_0}{I_1}$, where I_0 is the intensity of transmitted light (255) and I_1 is the intensity of the DAB-positive area of the sample.

TUNEL staining

Histologic sections were stained using TumorTACS™ *In Situ* Apoptosis Detection Kit (Trevigen) following manufacturer protocol.

Periodic acid Schiff staining

Samples were first deparaffinized with Histo-Clear and rehydrated in successive washes of 100%, 90%, and 75% ethanol, followed by a wash in deionized (DI) water. Slides were stained using the Periodic Acid Schiff Stain Kit (Abcam) following the manufacturer's protocol.

EdU treatment and tissue regeneration study

To evaluate DNA synthesis as a marker for epithelial regeneration, mice were given a single administration of 5-ethynyl-2'-deoxyuridine (EdU) by intraperitoneal injection at [200ug/kg] in PBS. Mice were sacrificed 2 hours after administration, with both small and large intestines prepared for histological analysis using Click-iT™ EdU Cell Proliferation Kit for Imaging, Alexa Fluor™ 488 (Thermo Fisher) according to manufacturer protocol.

Intestinal and MEF cell migration

To check cell migration in MEF, we performed a scratch wound assay. WT and KO MEFs were plated in a glass bottom tissue culture plate with a silicon spacer in the middle. Once cells adhered they were kept in a serum-starved medium overnight. The next day, the serum free medium was replaced by plus serum medium, and the spacer was gently removed. After 7 h, the cell migration was captured under a light microscope. The path traveled by the cells was analyzed using Fiji2 software.

Intestinal villi length was measured from the base to the apex using the Image J software segmented line tool. For each villus the length was subdivided into 3 equal sections (base, stem, apex), cells were counted and reported as per these subdivisions. For each subdivision, cell counts are reported as an average, by dividing the number of cells counted per subdivision by the total number of villi (*lpmk^{F/F}* 40, *lpmk^{4IEC}* 42).

CPT-11 treatment and tissue repair study

Mice were given a single administration of CPT-11 (Sigma) by intraperitoneal injection at 250 mg/kg in saline, in a total injection volume of 200 μ l. Mice were sacrificed 4 days post-injection as described above, with both small and large intestine taken for analysis.

Enteroid isolation from IPMK wild type and conditional knockout mice

Intestinal enteroids were isolated using a process adapted from STEMCELL Technologies protocol "Intestinal Epithelial Enteroid Culture with IntestiCult™ Enteroid Growth Medium (Mouse)." Mice were euthanized via CO₂ followed by surgical excision of the small intestine. Intestinal sections were gently flushed with cold DPBS and external membrane, blood vessels, and fat were removed. Intestinal segments were opened lengthwise and segmented into 2 mm sections which were then added to a 50 mL conical tube with cold DPBS. At this stage, the sections for each experimental group were combined. Intestinal fragments then underwent 15-25 cycles of washes in DPBS until the supernatant appeared clear. The DPBS was then replaced with room-temperature Gentle Cell Dissociation Reagent (GCDR) and left on a 25-rpm rocking platform for 20 minutes. Fragments were then resuspended in cold PBS with 0.1% BSA, after which the supernatant was collected and passed through a 70 μ m filter. This process of resuspension and filtration was repeated to create 5 fractions; each fraction was then centrifuged with pellets resuspended in cold DMEM/F12. Samples of each fraction were evaluated by light microscopy, and those with the highest proportion of intestinal crypts were selected for plating. Selected fractions were then centrifuged and resuspended in supplemented IntestiCult™ Enteroid Growth Medium with 100 mg/mL streptomycin. The resuspension was mixed with equal parts Matrigel® and plated on a pre-warmed 24-well plate. After 10 minutes, additional growth medium was added and Enteroid cultures were left to proliferate for 7 days. At this time, the Enteroids were passaged by first homogenizing the Matrigel domes in GCDR, followed by pelleting the Enteroids. GCDR was then aspirated and the pellet was resuspended in cold DMEM/F-12, followed by a second round of centrifugation. The pellet was then homogenized in IntestiCult Enteroid Growth Medium with 100 mg/mL streptomycin, combined with Matrigel, and re-plated as previously described. For inhibitor study enteroids were isolated and plated as described above. At the time of passaging, IntestiCult Enteroid Growth Medium was swapped with media containing 1 μ M GSK2334470 [PDK1 inhibitor] or AKT inhibitor VIII. Enteroids were harvested and sectioned 7 days after passaging.

Confocal microscopy

Images of adherent cells were acquired with a Zeiss LSM700 single-point, laser scanning confocal microscope. Histologic sections were imaged with both the Zeiss LSM700 as well as an ImageXpress Micro XLS widefield high-content analysis system. Images were analyzed with Zenlite, Imaris, and ImageJ software.

QUANTIFICATION AND STATISTICAL ANALYSIS

All plots and statistical analysis were performed with Prism 8 (GraphPad) software. Statistical significance was determined by either Student's t-test (two-tailed) for 2 groups or 1-way ANOVA for multiple groups with similar sample sizes. Error bars represent standard error of the mean, and n indicates number of experimental replicates or the number of animals employed. Differences between groups were considered significant when * $p < 0.05$, ** $p < 0.01$, and *** $p < 0.001$.